Industrial Crops & Products 212 (2024) 118304

Contents lists available at ScienceDirect

Industrial Crops & Products

journal homepage: www.elsevier.com/locate/indcrop

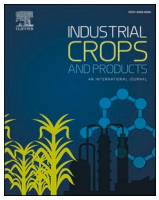

# Multiple approaches to exploit ferulic acid bio-based epoxy monomer for green thermoset

Lorenzo Pezzana [a], Eva Malmström [b,c], Mats Johansson [b,c], Valentina Casalegno [a], Marco Sangermano [a,*]

[a] Politecnico di Torino, Dipartimento di Scienza Applicata e Tecnologia, C.so Duca Degli Abruzzi 24, Torino 10129, Italy
[b] KTH Royal Institute of Technology, School of Engineering Sciences in Chemistry, Biotechnology and Health, Department of Fibre and Polymer Technology, Division of Coating Technology, Teknikringen 56-58, Stockholm SE-10044, Sweden
[c] KTH Royal Institute of Technology, School of Engineering Sciences in Chemistry, Biotechnology and Health, Department of Fibre and Polymer Technology, Wallenberg Wood Science Centre, Teknikringen 56-58, Stockholm SE-100 44, Sweden

ARTICLE INFO

*Keywords:*
Ferulic acid
Thiol-epoxy
UV-curing
Bio-based monomer
Cationic
Thiol-ene

ABSTRACT

Bio-based monomers are under investigation to replace fossil-based materials due to the concerns regarding climate change and depletion of fossil raw materials. Lignin, cellulose and hemicellulose represent the main interesting platform to use for developing new monomers due to their significant abundance. Ferulic acid is one of the moieties derived from lignin which can be suitable for many applications. In this study, the ferulic acid was epoxidated and it was investigated in cationic UV-curing. Due to the limited performance obtained during UV-curing, two alternative strategies were developed to overcome the initial problem of poor material properties. A thiol-ene epoxy system based on the ferulic epoxy derivative and a commercially available thiol as well as a thermally cured system based on pure cationic curing of ferulic acid diepoxy were chosen as alternative methods. The different curing processes were thoroughly investigated by means of FTIR (Fourier transform infrared spectroscopy) and photo-DSC (differential scanning calorimetry). The thermo-mechanical properties of the thermosets employing DMA- (dynamic mechanical analysis) and tensile analysis were deeply evaluated. Finally, the possibility to use the best cured system as an adhesive was raised investigating the shear strength of metallic and composite joined samples using the single lap offset (SLO) test under compression.

## 1. Introduction

Biobased monomers are playing a central role to replace commercially available fossil-based resins used in several thermoset applications (Bozell and Petersen, 2010; John et al., 2019). Cellulose, hemicellulose and lignin are the main biopolymers present in different bio-sources, from plant to grass. They are the platforms for new green monomers (Alén, 2015; Gandini and Lacerda, 2015; Rajesh Banu et al., 2021). The large availability of the main sources and the high amount of waste derived from food chain and agricultural processes, such as pulp and paper, generate a feasible path to pursuit in order to obtain valuable chemicals (Chavan et al., 2018; Ioannidou et al., 2020; Jha and Kumar, 2019).

The scientific community is continuously studying the possibilities to exploit vegetable oils (Gandini and Belgacem, 1998), furan-derivatives (Gandini, 2008; Yue and Queneau, 2022), isosorbide-based monomers (Ma et al., 2016), terpenes (Silvestre and Gandini, 2008a; Wilbon et al., 2013), rosins (Chen, 1992; Kugler et al., 2019; Silvestre and Gandini, 2008b) and cinnamic acid (Fonseca et al., 2019) as polymeric precursors.

In view of sustainability, a main role is also played by the process employed to obtain the final materials. UV-curing has been reported to have several advantages with respect to classical thermal curing. Fast curing, mild conditions, absence of VOCs emission are some of the advantages (Pezzana et al., 2022b; Sangermano et al., 2014; Yagci et al., 2010). However, most of the monomers derived from natural sources are missing photocurable reactive groups, thus functionalization is required to obtain an UV-active monomer useful in curable resins.

Cationic UV-curing requires the exploitation of vinyl- or epoxy-functionalities (Decker, 2002; Stanford et al., 2001). Epoxy resins exhibit high glass transition, good tensile properties and thermo-mechanical stability thus several works investigate the use of

* Corresponding author.
*E-mail address:* marco.sangermano@polito.it (M. Sangermano).

https://doi.org/10.1016/j.indcrop.2024.118304
Received 24 November 2023; Received in revised form 4 February 2024; Accepted 22 February 2024
Available online 2 March 2024

these compounds for a range of applications, covering various fields from coatings to adhesives (Auvergne et al., 2014). In the last years, the bio-based epoxies are currently under investigation to substitute fossil-based resin counterparts. Epoxy-functional vegetable oils (Noè et al., 2021), furan monomers (Pezzana et al., 2021; Pezzana et al., 2023, 2022a, 2022b), lignin-based monomers (Silau et al., 2022; Ye et al., 2021) reveal outcomes comparable with traditional fossil-based thermosets.

The epoxy-unit can be also employed for thiol-epoxy networks exploiting the reaction between an oxirane ring and a thiol group generating a β-hydroxythio-ether linkage (Carioscia et al., 2007; Konuray et al., 2018; Stuparu and Khan, 2016). The reaction is catalyzed by a base, which under heating or UV-irradiation, generates a thiolate anion that opens the epoxy ring (Konuray et al., 2017a). The thiol–epoxy reaction is strongly autocatalytic due to the concurrent base formation that facilitates the ring-opening reaction (Jin et al., 2015). One of the main drawbacks is the short storage stability of the formulations, so photo-latent based compounds have been proposed to enhance the stability of the formulation, allowing to start the reaction by an external trigger such as irradiation by UV-light (Chen et al., 2020; Konuray et al., 2017b). Thiol-epoxy networks have been employed for several applications also in combination with thiol-ene or thiol-acrylate system to generate strong networks (Carioscia et al., 2007; Guzmán et al., 2015; Sangermano et al., 2010). They have been used for shape memory polymers (Belmonte et al., 2015) and for polymers with tunable surface properties (Romano et al., 2018). Lately, thiol-epoxy networks have been used to produce new biobased thermosets based on eugenol (Guzmán et al., 2018, 2017), gallic acid and vegetable oils (Feng et al., 2019).

Among the different bio-based sources, ferulic acid (FA) is very interesting because of its chemical structure; it is a hydroxy cinnamic acid owing three different functional groups; an acid, a phenol, and a double bond which can be explored for further functionalizations (Alexakis et al., 2023; Fonseca et al., 2019). Moreover, it has an aromatic ring that increases the rigidity of the structure, improving the properties of the derived network (Rosazza et al., 1995). FA is one member of the cinnamic acids together with caffeic and sinapic acid (de Oliveira et al., 2015; Kumar and Pruthi, 2014). FA is present in lignin, the second most abundant biopolymer after cellulose and it plays a central role in the plant cell structure (Alén, 2015; Cazacu et al., 2012). FA can be produced by enzymatic synthesis (Fang et al., 2023; Uraji et al., 2013) to become available for production of chemicals or supply of energy generating green fuels such as ethanol (de Oliveira et al., 2015). FA has been studied to substitute phthalic acid for thermoplastic applications (Mialon et al., 2010; Pion et al., 2014). Moreover, it has been used as an interesting building block for polyurethanes, epoxies, and phenolic resins (Kreye et al., 2011; Llevot et al., 2016; Ménard et al., 2017). Recently it has been employed for thermoset applications with a furan-derivative to produce thermosets with high $T_g$ due to the high cross-link density achieved by thermal curing (Ye et al., 2021). It has also been used for the production of a polymeric network with vitrimeric properties (Zhong et al., 2022). FA has been already exploited in UV-curing in thiol-ene system highlighting the possibility to tailor the final properties according to the chemical structure. In this case, the free radical UV-curing was possible due to the allylation step done on FA, creating the bi-functional ene monomer useful for the radical photopolymerization (Pezzana et al., 2021).

There is a growing need to expand the synthetic toolbox that enables the facile transformation of biobased compounds into highly reactive monomers to compete with the commercially available resins which had a main role in the worldwide market. In this framework, FA was identified as a starting monomer to synthesize an epoxy-derivative useful for the development of thermosets employing UV-activated curing techniques. Considering epoxidized FA, the investigation focused on its reactivity in cationic UV-curing. Because of the limited success of the reactions, the exploitation of epoxidized FA persuaded following two possible strategies moving toward a thiol-epoxy UV-activated reaction and a thermal cationic curing to produce the final thermosets. Scheme 1 reports the three different approaches used in this study to achieve bio-based thermosets. Considering the thiol-epoxy system, a further investigation about the possibility to tailor the final properties of the thermoset playing with the thiol-epoxy ratio was carried out. The different curing processes were deeply analyzed, employing ATR-FTIR (attenuated total reflectance Fourier transform infrared spectroscopy), photo-DSC (dynamic scanning calorimetry), DSC, and photorheology analyses. Different thermosets were produced following the different approaches and the thermo-mechanical properties of the cross-linked networks were well characterized. The thermally-cured networks were proposed for bio-based adhesive materials. Finally, the chemical degradation of the thermosets in an alkaline environment was assessed.

## 2. Materials and methods

### 2.1. Materials

Ferulic acid (FA 99% purity), epichlorohydrin (ECH), tetrabutylammonium bromide (TBAB), sodium hydroxide, trimethylolpropane tris(3-mercaptopropionate) (TMPMP), ytterbium(III) trifluoromethanesulfonate (YTT, 99% purity), and triarylsulfonium hexafluoroantimonate salts (S-Sb) mixed in propylene carbonate were purchased from Sigma Aldrich. The photolatent base 4-(hexahydropyrrolo[1,2-*a*]pyrimidin-1-ylmethyl)-benzoic acid methyl ester (PLB) was supplied from BASF. Magnesium sulphate ($MgSO_4$) was acquired from Acros Organic. Ethyl acetate and heptane were supplied by VWR Solvent. NMR analysis was performed with deuterated chloroform ($CDCl_3$) provided by VWR Chemicals.

### 2.2. Synthesis of ferulic acid-based diepoxy (FAE)

The epoxidation was performed combining previous protocols as presented in Scheme 2 (Ye et al., 2021; Zhong et al., 2022). Ferulic acid (FA 15 g, 77 mmol) was mixed with ECH (10 equivalent, 71 g) and TBAB as catalyst (0.01 equivalent, 0.25 g) in a three-necked flask equipped with a magnetic stirrer. The mixture was heated at 105 °C under reflux for 2 h. Then the solution was cooled down to room temperature. The mixture was then further cooled down at 0 °C in an ice bath and a water solution of NaOH 40 wt% was added to the mixture employing an adding funnel (100 mL). The solution was kept under stirring for 3 h. The organic phase was extracted three times with ethyl acetate (30 mL) then the collected phases were washed six times with water (30 mL). After removal of water by drying with $MgSO_4$, the solvent was evaporated to obtain a yellow liquid. The last traces of ECH were removed by precipitation of the liquid in heptane (50 mL). The precipitation was repeated two times. The ferulic acid based diepoxy (FAE) was collected as a white solid and dried overnight in vacuum (16.5 g, yield: 70%).

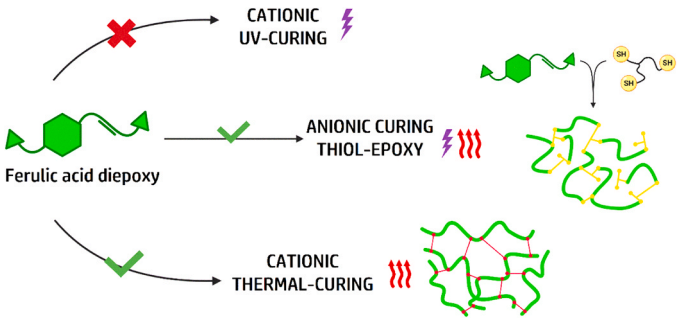


**Scheme 1.** Approaches used in the study for exploiting curing of the epoxidized ferulic acid.

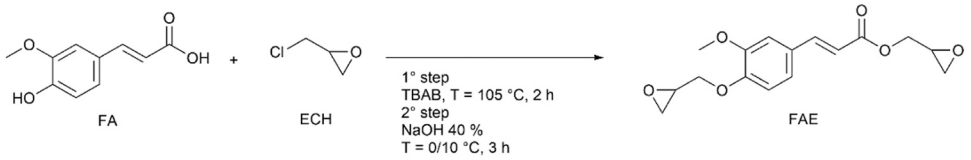


**Scheme 2.** Epoxidation of ferulic acid (FA) using epichlorohydrin under alkaline conditions.

$^1$H NMR (400 MHz, $CDCl_3$) δ 7.67 (d, $J$ = 16.0 Hz, 1 H), 7.14 – 7.03 (m, 2 H), 6.93 (d, $J$ = 8.3 Hz, 1 H), 6.35 (d, $J$ = 15.9 Hz, 1 H), 4.56 (dd, $J$ = 12.3, 3.0 Hz, 1 H), 4.31 (dd, $J$ = 11.4, 3.3 Hz, 1 H), 4.10 – 4.01 (m, 2 H), 3.91 (s, 3 H), 3.44 – 3.25 (m, 2 H), 2.98 – 2.86 (m, 2 H), 2.74 (ddd, $J$ = 23.8, 4.9, 2.6 Hz, 2 H).

$^{13}$C NMR (101 MHz, CDCl3) δ 166.90, 150.32, 149.78, 145.50, 128.16, 122.66, 115.51, 113.45, 110.41, 70.12, 65.08, 56.08, 50.18, 49.68, 44.99, 44.86.

### 2.3. Curing of ferulic acid diepoxy

FAE was used in three different formulations listed in Table 1 allowed for three different types of curing.

The FAE was melted (around 80 °C) and then it was mixed with the triarylsulfonium hexafluoroantimonate (S-Sb, cationic photoinitiator) in 2 wt% and UV-cured in a silicon mold (12×8x0.2 mm$^3$). The UV-source was a UV-DMAX Flood lamp equipped with a static mercury lamp with an emission spectrum between 600 and 250 nm centered around 365 nm and a light intensity of about 100 mW/cm$^2$. This allowed to generate sample *via* UV cationic curing for further analysis. The samples were irradiated for 2 min.

The thiol-epoxy system was obtained by mixing FAE with TMPMP in a stochiometric ratio (epoxy:thiol functionality). For clarity the formulation is denoted as FAE:SH,2:3, due to the reactive groups of FAE (2 epoxies) and TMPMP (3 thiols), respectively. The photolatent base (PLB) was then added (2 wt%) and the formulation was cured under the UV lamp (100 mW/cm$^2$) for 2 min in silicon molds, either with a rectangular shape (12×8 mm$^2$, with thickness of 0.2, 0.4, and 1 mm) or dog-bone shape for tensile test. Moreover, a further formulation with equimolar amounts of epoxy and thiol groups was produced and analyzed. In this case the formulation is denoted FAE:SH,3:3 due to reactive groups considered for each monomer, FAE (2 epoxy and 1 carbon-carbon double bond, 3 total) and TMPMP (3 thiols).

Finally, FAE was mixed with YTT (2 wt%) as a thermal cationic initiator whereafter the samples were thermally cured in silicon molds at 150 °C for two hours and 180 °C for another 2 h to ensure complete curing. The sample were in rectangular shape for DMA-analysis (12×8x0.4 mm$^3$), and dog-bone shape (type 5B) for tensile tests. With this formulation further adhesive tests were performed.

### 2.4. Methods

#### 2.4.1. Nuclear magnetic resonance (NMR)

NMR analysis was performed by means of a Bruker AM 400. $^1$H NMR and $^{13}$C NMR spectra were recorded at 400 MHz and 101 MHz respectively. $CDCl_3$ was used as internal reference and solvent.

**Table 1**
Formulations tested in this study.

| ENTRY | Epoxy monomer | Thiol monomer | Initiator | Curing |
|---|---|---|---|---|
| FAE | FAE | - | S-Sb (2 wt %) | UV |
| FAE: SH,2:3 | FAE | TMPMP (ratio 2:3) | PLB (2 wt %) | UV + thermal |
| FAE: SH,3:3 | FAE | TMPMP (ratio 1:1) | PLB (2 wt %) | UV + thermal |
| FAE_YTT | FAE | - | YTT (2 wt %) | Thermal |

#### 2.4.2. Fourier transform infrared spectroscopy (FTIR)

A Nicolet iS 50 Spectrometer was employed for the characterization of the UV-process. Data were collected in ATR mode with 32 scans with a spectral resolution of 4.0 cm$^{-1}$. All data were recorded with the software Omnic from Thermo Fischer Scientific. The epoxy was evaluated taking into account the signals at 905 and 855 cm$^{-1}$; the thiol was evaluated by the vibration band located at 2750 cm$^{-1}$ and the double bond was monitored at 1640 cm$^{-1}$.

#### 2.4.3. Photo-differential scanning calorimetry (Photo-DSC & DSC)

The photo-DSC analysis was performed on a Mettler Toledo DSC-1 equipped with Gas Controller GC100. A Hamamatsu LIGHTINGCURE LC8 was the light source. It was equipped with a mercury lamp and an optic fiber directed the UV-irradiation on the formulation. The formulation was placed in an open aluminum pan while an open empty pan was used as references and the irradiation was simultaneously directed on the pans. The method required two steps of irradiation separated by a stabilization step in order to investigate the completeness of the UV-curing process of a liquid formulation. The second step aimed to create the base line of the method since no exothermic peak are visible in case of complete UV-curing. Indeed, the final curve is the result of the subtraction between the two UV steps. The thiol-epoxy system was studied at different temperatures (25, 50, 75, and 100 °C) to investigate the UV-curing. Moreover, isothermal analysis of one hour at the selected temperature without UV-irradiation was performed to reveal the influence of temperature during cure. The thiol-epoxy conversion for the FAE_SH formulations and the epoxy conversion of FAE_YTT system achieved by thermal curing were calculated by Eq. 1.

$$Conversion = \frac{\Delta H_{\exp}}{\Delta H_{dynamic}} \tag{1}$$

where $\Delta H_{exp}$ is the enthalpy registered in the isocuring condition and $\Delta H_{dynamic}$ is the enthalpy evaluated in the dynamic run performed from 25 to 300 °C which can theoretically guarantee complete curing. Thus, it can be taken as references to evaluate the conversion.

Finally, the dynamic curing was performed on epoxy formulation containing YTT. Heating rates of 2, 5, 10 or 20 K/min, respectively, were applied from 25 to 300 °C. The isothermal curing study was conducted at 150, 160, 170, and 180 °C and Eq. 2 was used to describe the curing process (Criado et al., 1989) and Eq. 3 was used to derive the activation energy of the curing process (Kissinger, 1957; Yoo et al., 2010).

$$\frac{d\alpha}{dt} = Ae^{-\frac{E_a}{RT}}f(\alpha) \tag{2}$$

where $\alpha$ is the fraction of the conversion, $t$ is the curing time, $d\alpha/dt$ is the conversion rate, $A$ is the preexponential factor, $E_a$ is the activation energy, $R$ is the gas constant, $T$ is the absolute temperature. Eq. 2 represents the kinetic model for the evaluation of the thermal curing.

$$\frac{d\left[\frac{\ln(\phi)}{T_p^2}\right]}{d\left(\frac{1}{T_p}\right)} = -\frac{E_a}{R} \tag{3}$$

where ϕ is the heating rate (°C/min) and $T_p$ is the maximum in the dynamic DSC curve. From the slope of the Arrhenius plot the $E_a$ can be determined.

The DSC was also performed on UV-cured thermoset and thermally cured ones to investigate the thermal behavior of the different thermosets. The method used for the investigation was divided in different steps. Firstly, heating from 25 to 100 °C which eliminate the thermal history; then the chamber was cooled until – 40 °C, finally the $T_g$ was identified by a second heating until 250 °C. The heating and the cooling rates were set at 10 °C/min and the analysis was performed in a nitrogen atmosphere with a flow rate 40 mL/min. In this study 40 μL aluminum pans were used. The data were handled with Mettler Toledo STARe software V9.2.

#### 2.4.4. Photorheology

The instrument Anton Paar MC 302 was used to investigate the UV-curing process. The light source was a Hamamatsu LIGHTINGCURE LC8 lamp which was equipped with an optic fiber to irradiate the sample. The intensity of the UV-light was 40 mW/cm$^2$. The tests were performed with a plate-plate geometry; the upper metal accessory had a diameter of 2.5 cm while the bottom plate was a quartz disk to ensure the irradiation on the sample. The distance between the crystal and the plate was 200 μm which corresponds approximately to 150 μL of coating resin. The frequency was 1 Hz, with a strain of 1% and the lamp was switched on after 60 seconds which were used to ensure initial stability to the system.

#### 2.4.5. UV–vis spectroscopy

A Jenway 6850 UV/Vis Spectrophotometer was used to investigate the absorbance of the bio-based monomer. The spectra were recorded from 600 nm to 200 nm using quartz cuvette. Acetonitrile was used as solvent and different concentrations of FAE were tested.

#### 2.4.6. Dynamic mechanical thermal analysis (DMTA) and evaluation of crosslinking density

The DMTA analysis was performed with a Triton Technology instrument. The analysis investigates the trend of the Storage Modulus ($E'$) and Tan δ as a function of temperature. The tests were started at – 40 °C ensured by cooling down the test chamber with liquid nitrogen. Tensile mode was used to perform the measures applying a tensile stress frequency of 1 Hz and a displacement of 0.02 mm. The measurements were stopped after the appearance of the rubbery plateau detected in the storage modulus. The peak of *Tanδ* indicate the $T_g$ of the polymer network. The analyzed samples had an average dimension of 0.4 ×8×12 mm$^3$. Eq. 4 is taken from the statistical theory of rubber elasticity providing an estimation of the density of cross-links.

$$\nu_c = \frac{E'}{3RT} \tag{4}$$

where $\nu_c$ is the number of crosslinks per volume of the crosslinked network, $E'$ is the storage modulus in the rubbery plateau ($T_g + 50$ °C), $R$ is the gas constant and $T$ is the temperature in Kelvin.

#### 2.4.7. Tensile test

The tensile test (ASTM D638) was performed on a 5B type dog-bone samples (with $l_0 = 12$ mm and $A_0 \approx 3$ mm$^2$). The stress-strain curves were registered using a MTS QTestTM/10 Elite. The data were handled with a measurement software (TestWorks® 4, MTS System Corporation). The load cell of 500 kN was used; the cross-head speed of the machine was set as 5 mm/min. The Young's modulus ($E$) was evaluated as the slope of the curve up to the linear region (about 20% of total reached elongation). The results were the average value from at least five measurements.

#### 2.4.8. Mechanical joint characterization

The thermally cured FAE in the presence of YTT was tested for adhesive applications. Different substrates of aluminum, CMC composite and steel were used to analyze the adhesion. Aluminum was a precipitation-hardened EN AW-6082 T6 alloy; CMC was a carbon short-fiber reinforced core material. This core material undergoes a liquid silicon infiltration process after the manufacturing of the green body and pyrolysis. During this infiltration, an *in-situ* reaction takes place between silicon and carbon, leading to the formation of silicon carbide. As a result of this process, the silicon infiltration leaves behind a porosity ranging from 0.5% to 3.0%. Upon completion of the manufacturing process, the CMCs consist of a mixture of free silicon, silicon carbide, and carbon, as both carbon fiber and residual pyrolytic carbon, in a 15, 50, and 35% ratio respectively. The steel was an AISI 441. The substrates were cut into a rectangular shape (~ 25 ×25 mm$^2$) and they were joined in a single shear-lap test according to Scheme 3. The surfaces of the substrate were polished to guarantee uniformity in the contact between surface and adhesive. A polishing machine, equipped with sandpaper (400 grit), was used and after the polishing treatment, substrates were sequentially rinsed in a sonic bath with ethanol. A spatula was used to apply the adhesive on the facing surfaces, ensuring a sufficient amount of mixed adhesive was used to achieve an appropriate thickness for the final adhesive bond area. The adhesive thickness was range between 0.2 and 0.3 mm and the area of the joint was about half of the length of the substrate (~ 12 ×25 mm$^2$). The thickness of the joint was derived measuring the thickness of the total piece subtracting the thickness of the two substrates. The curing was done as previously described in the Paragraph 2.3. at 150 °C for two hours and then 180 °C for other two hours, then the samples were left to reach room temperature. The shear strength was evaluated by applying Eq. 5 where *Load* was the maximum force applied on the joint while the *Adhesive area* was the area of the glue joint.

$$\tau = \frac{Load}{Adhesive \quad area} \tag{5}$$

The mechanical strength (apparent shear strength) of the joined samples was assessed through a single lap offset (SLO) test conducted under compression at room temperature. The testing method employed was adapted from the ASTM D1002–05 standard, utilizing the universal testing machine SINTEC D/10 with a cross-head speed of 0.5 mm/min. At least five samples were tested for each similar joint (i.e steel-to -steel, CMC to CMC, aluminum-to-aluminum). The results of the mechanical tests were expressed as mean ± standard deviation.

#### 2.4.9. Chemical hydrolysis study

The degradation study was conducted in an alkaline environment (NaOH 2 M). Cured samples of about 100 mg were weighed ($W_i$), then immersed into the solution and stirred at room temperature at 120 rpm for two months. After a selected time, the samples were removed from the solution, rinsed with deionized water, dried in an oven at 50 °C over night to ensure correct mass measurements during degradation and finally weighed ($W_t$). Eq. 6 was used to evaluate the time-dependent degradation comparing the difference in the weight before and after the immersion in the alkaline solution.

$$Weight(\%) = \frac{W_t}{W_i} \times 100 \tag{6}$$

## 3. Results and discussion

### 3.1. Synthesis of epoxidized ferulic acid and cationic UV-curing

The FA epoxidation was achieved following previous protocols reported in literature (Ye et al., 2021; Zhong et al., 2022) obtaining FAE in relatively high yield and purity, as confirmed by NMR analysis (Fig. 1). The high scalability of the protocol allowed to obtain the required

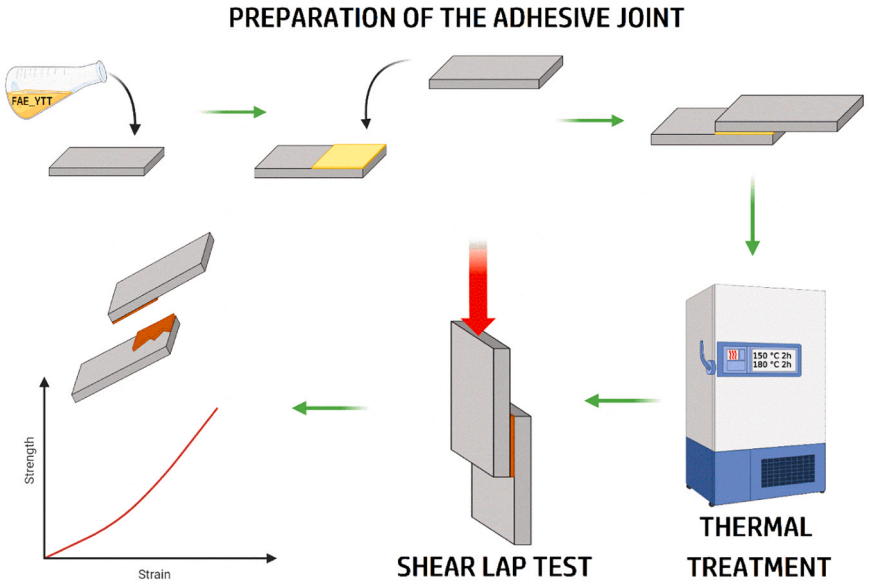


**Scheme 3.** Preparation and testing of the joints. The different steps are shown from the spreading of the formulation on the substrate to the final shear lap test.

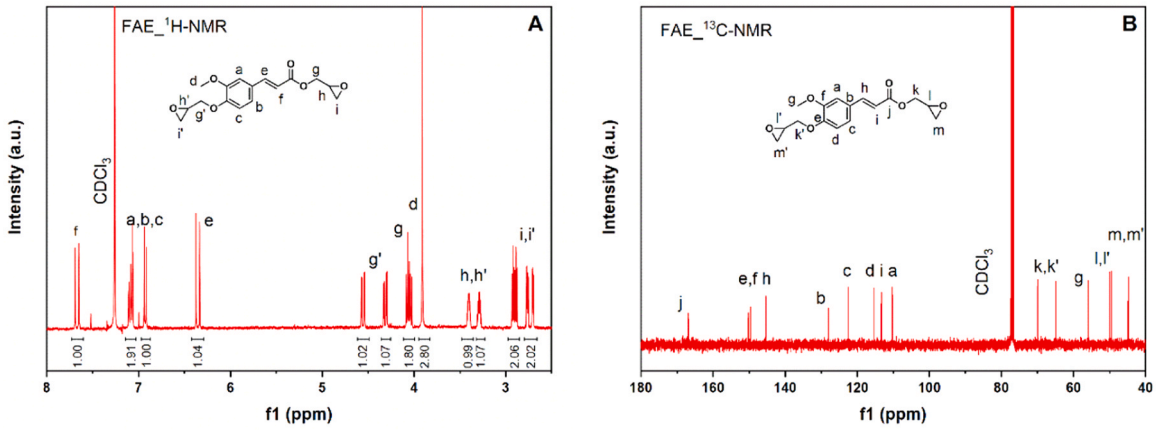


**Fig. 1.** (A) $^{1}$H NMR and (B) $^{13}$C NMR spectra of the synthesized FAE.

amount of product for the further analysis. This involved the use of ECH as epoxidation reagent, that could represent a limitation in green level of the entire process (Çavuşoğlu and Yalçin, 2023), nevertheless at this moment this reagent is crucial to achieve the epoxidation of several monomers (Caillol et al., 2021; Eid et al., 2021; Pezzana et al., 2021; Xin et al., 2016). Future studies could be performed to avoid the hazardous ECH, scouting for greener processes to increase the sustainability of this established class of monomers (Sternberg et al., 2021).

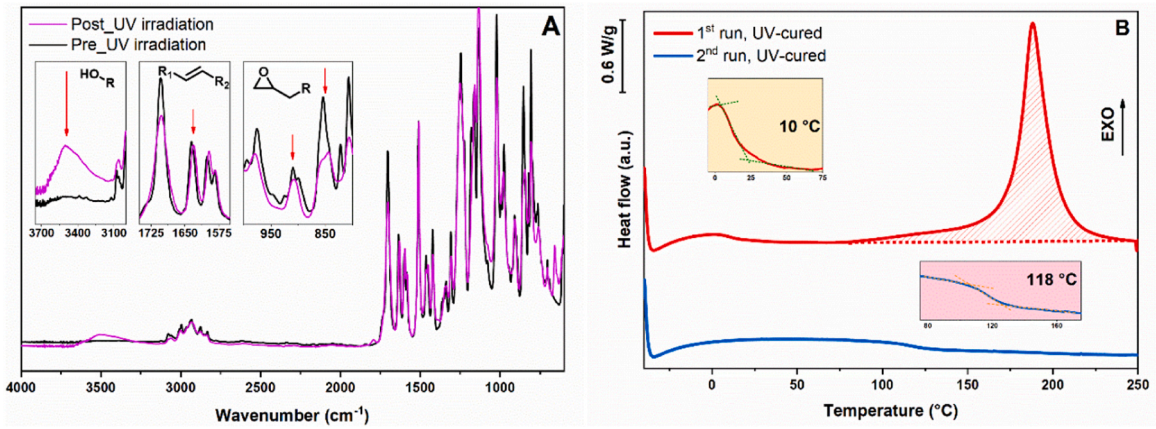


**Fig. 2.** ATR-FTIR pre and post UV-irradiation and DSC of UV-cured FAE.

The cationic UV-curing of FAE was investigated in the presence of sulphonium salt as photoinitiator. The UV-irradiation was not completely successful achieving only a partial curing as confirmed by ATR-FTIR and DSC analysis (Fig. 2). The epoxy vibration bands centered at 905 $cm^{-1}$ and 855 $cm^{-1}$ were slightly reduced confirming partial/incomplete reaction. However, the opening of the epoxy ring was confirmed by the appearance of OH band at 3500 $cm^{-1}$. As expected, the C═C double bond was not affected and remained unchanged as confirmed by the band at 1640 $cm^{-1}$. The DSC analysis performed on a UV-cured sample, showed a $T_g$ around 10 °C and an exothermal peak present around 150 °C due to the incomplete curing reaction. From this analysis it was also possible to investigate the theoretical $T_g$ achievable with the thermal treatment. Indeed, the second thermogram reported in Fig. 2 highlighted a higher $T_g$, at around 120 °C. This was due to the thermal degradation of the photoinitiator which started the epoxy curing at high temperature allowing a complete cross-linking reaction.

The partial cross-linking was also confirmed by photorheological analysis as presented in Figure S1. In this analysis the monitoring of the storage modulus evidenced an increase in the $E'$ value due to the cross-linking reaction with an evident delay in the time and the achieved storage modulus value was in the order of $10^3$ Pa. This value was relatively low compared with the usual value of around $10^5$-$10^6$ Pa and was attributed to the low epoxy group conversion.

The limitation of the curing was explained analyzing the UV–vis spectra of the FAE (Fig. 3) where an extremely broad and intense absorption peak between 200 and 400 nm can be observed. This absorption competes with the absorption of the cationic photoinitiator, severely limiting the efficiency of the process. Moreover, the penetration depth of the light can also be limited due to the strong monomer absorption.

Thus, it is possible to affirm that the intrinsic chemical nature of the starting monomer is a limiting factor for the exploitation of cationic UV-curing process. However, to overcome this challenge, the system was redesigned by adopting two different possible solutions: firstly, a thiol-epoxy system activated by a photo-latent base initiator and secondly, a cationic thermal-curing activated by an Ytterbium initiator.

### 3.2. Thiol-epoxy anionic curing

Thiol-epoxy anionic curing systems are activated by UV-light, resulting in the formation of a strong base originating from the photo-latent base (PLB) (Romano et al., 2018). PLB deprotonates the thiol group and the generated anion opens the epoxy ring to a achieve a thiol-epoxy cross-linked network (Reisinger et al., 2022). Thus the reaction can be considered “click chemistry” due to ratio 1:1 between the opening of the epoxy-ring and the reaction of a thiol group

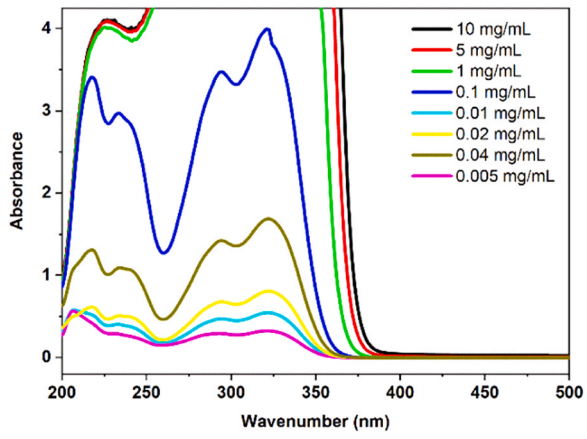


**Fig. 3.** UV–vis spectra of the FAE at different concentrations. The measurements were conducted in acetonitrile.

(Fernández-Francos et al., 2016; Konuray et al., 2017a, 2017b, 2020).

The cross-linking process was monitored by ATR-FTIR analysis. Fig. 4A reports the spectra pre- and post- irradiation for the formulation containing a stochiometric ratio between the epoxy- and the thiol-groups. Following the ATR-FTIR analysis, the disappearance of the vibration bands related to epoxy and thiol groups confirmed the occurrence of the thiol-epoxy click reaction. Moreover, an increase in the region originating from hydroxyl groups was also detected, due to the ring opening of the epoxy-ring. Lastly, a decrease in the C═C signal was also observed, possible due to the thiol-ene reaction. Scheme 4 reports the UV-activation step of the PLB and the thiol-epoxy and thiol-ene reactions which happen in the studied system. Thus, we decided to use an excess of thiol taking into consideration that thiol-groups under UV-irradiation can also promote the thiol-ene reaction with the double bond of epoxidized ferulic acid besides participating to the thiol-epoxy cross-linking reaction promoted from the photolatent base. Previously, a work reported the possibility that the C═C double bond present into the ferulic monomer structure can react by thiol-ene reaction (L Pezzana et al., 2021). In this new system, this fact was further confirmed by analyzing a new formulation containing a 1:1 ratio between the thiol- and the functional groups of the FAE, i.e. FAE:SH,3:3. This assumption was done considering three reactive group in FAE, two epoxy groups and one C═C double bond. The ATR-FTIR of the resulting thermoset (Fig. 4B) and the reactivity of the C═C double bond was confirmed by the disappearance of the C═C vibration band. The decrease was more accentuate with respect the formulation with stochiometric ratio between epoxy and thiol (Fig. 4A) meaning and higher contribute of thiol-ene cross-links.

The investigation of the curing process pursued with photo-DSC analysis. Taking into consideration that the heating is required for the mixing of the formulations, the influence of the temperature on the curing was investigated. It is demonstrated that the thiol-epoxy reaction can be triggered by heat or UV-irradiation (Chen et al., 2020; Konuray et al., 2017b) thus the influence of the two components was assessed by photo-DSC analysis and isothermal curing. The Fig. 5 reports the analyses performed on the formulations with stochiometric ratio between epoxy and thiol, FAE:SH,2:3. It can be noticed that the UV-light had a beneficial effect on the overall reaction time, reducing it from hours to minutes (Fig. 5A). Nevertheless, the rate of polymerization was increased significantly with UV-irradiation; the height of the peak at 100 °C increased about 5 times when the formulation was UV-irradiated (Fig. 5C). However, it was found that the temperature played a crucial role in the activation of the reaction as confirmed by isothermal curing conducted at 60, 80, and 100 °C respectively. The temperature increment itself of the curing temperature from 60 to 100 °C meant a significative reduction of reaction time. The consequence was a direct increase in the speed of the reaction as can be clearly seen in Fig. 5B.

The monomer conversion was evaluated by taking the dynamic curing as a reference for a complete curing (Figure S2). The FAE:SH,2:3 had a total enthalpy of 528 ± 16 J/g while FAE:SH,3:3 had 394 ± 15 J/g.

Conversion curves were derived from DSC thermograms for the FAE:SH,2:3 (Figure S3). It is clear that the UV-irradiation was beneficial to activate the PLB, and hence thereby accelerating the cross-linking reaction. All the data from DSC analyses are listed in Table 2. The DSC thermogram for the FAE:SH,3:3 is reported in Figure S4 which confirmed the same trend showed for the previous formulation. Furthermore, the conversion vs time plot (Figure S5) corroborated and confirmed the analysis carried out for FAE:SH,2:3, revealing a decrease of the total time of the reaction by using UV.

The DMA analysis performed on the thiol-epoxy system revealed that the different ratio between TMPMP and FAE had an interesting impact on the final properties. FAE:SH,2:3 (epoxy:thiol = 1:1) resulted in the highest $T_g$, 47 °C while the FAE:SH,3:3 had a $T_g$ of 30 °C (Fig. 6). This can be explained considering the high impact of thiol-ene network. In the FAE:SH,2:3 system, the thiol-epoxy reaction prevailed contributing to

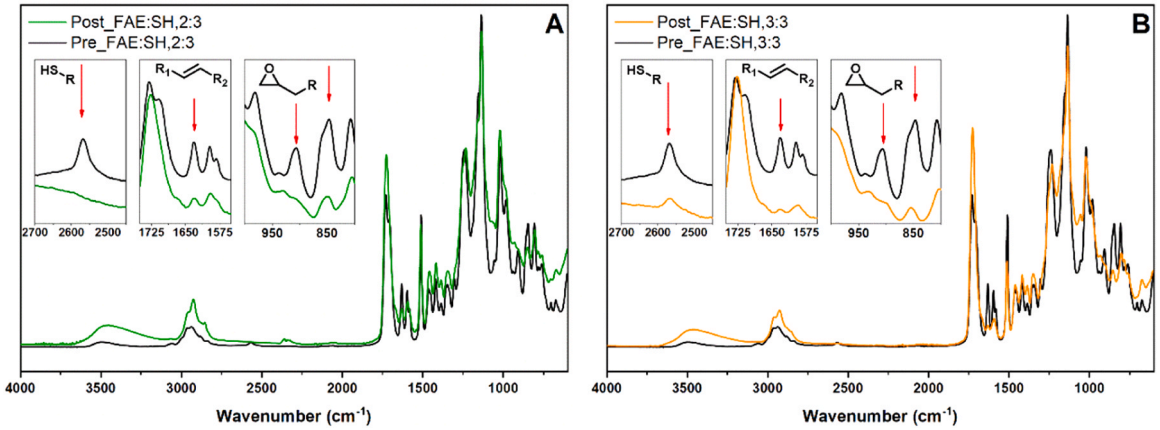


**Fig. 4.** (A) ART-FTIR of FAE:SH,2:3 (black and green) and (B) FAE:SH,3:3 (black and orange) pre and post irradiation with the highlights of the main changes in the vibration bands of the reactive groups involved into the cross-linking.

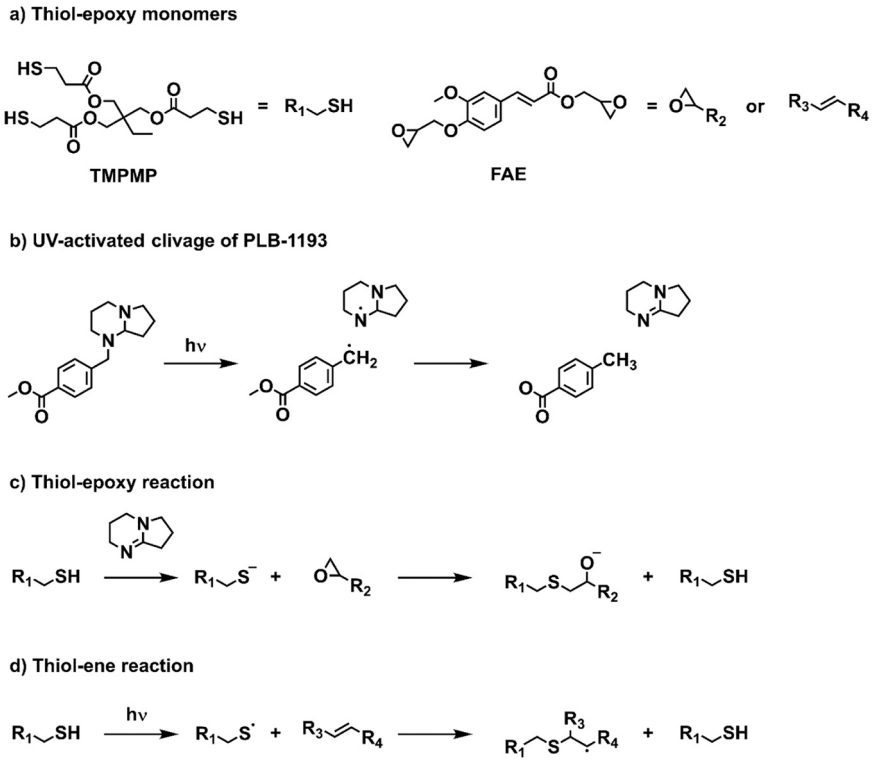


**Scheme 4.** Reaction scheme of the studied system with highlighted the monomers used in the formulation (a), the activation mechanism of PLB (b), the thiol-epoxy reaction (c), and thiol-ene reaction (d).

higher $T_g$ as compared with FAE:SH,3:3 where thiol-ene dominated. It is known that the thiol-ene systems usually have a low $T_g$, close to room temperature (Pezzana et al., 2021; Pezzana and Sangermano, 2021). Thus, a higher contribution from this specific type of bond to the thermoset can contribute to reducing the final $T_g$. All the DMTA data were corroborated and confirmed by DSC-analysis performed on cured samples; the results are reported in Figure S6.

Tensile analysis was carried out to investigate the mechanical properties of thiol-epoxy systems. The FAE:SH,2:3 had higher mechanical response than FAE:SH;3:3, especially it reached higher $E$ and σ. The FAE:SH,3:3 had the highest elongation at break, possibly due to the lowest $T_g$ which was close to the tested temperature affecting the behavior. Indeed, the high elastic elongation could be explained considering that the polymer network is mainly in the rubbery region (as DMTA analysis confirmed). The FAE:SH,3:3 had the lowest modulus and strength at break due to its chemical composition and less cross-link bonds ($\nu$ = 52 mmol/dm$^3$) compared with FAE:SH,2:3 with had a cross-link density of 85 mmol/dm$^3$. Moreover, the cross-links were mainly composed by S-C linkage derived from thiol-ene reaction in the FAE:SH,3:3 while the FAE:SH,2:3 presented main β-hydroxythio-ether linkages derived from thiol-epoxy reaction which could have increased the rigidity of the network. All the curves are presented in Figure S7.

### 3.3. Cationic thermal curing

The last part of the investigation of the curing process exploited the use of the ytterbium-containing compound YTT as thermal cationic initiator. Therefore, the FAE was mixed with YTT and thermally cured at 150 °C for two hours followed by 2 h at 180 °C. The efficiency of this particular type of initiator has been already proven for the thermal

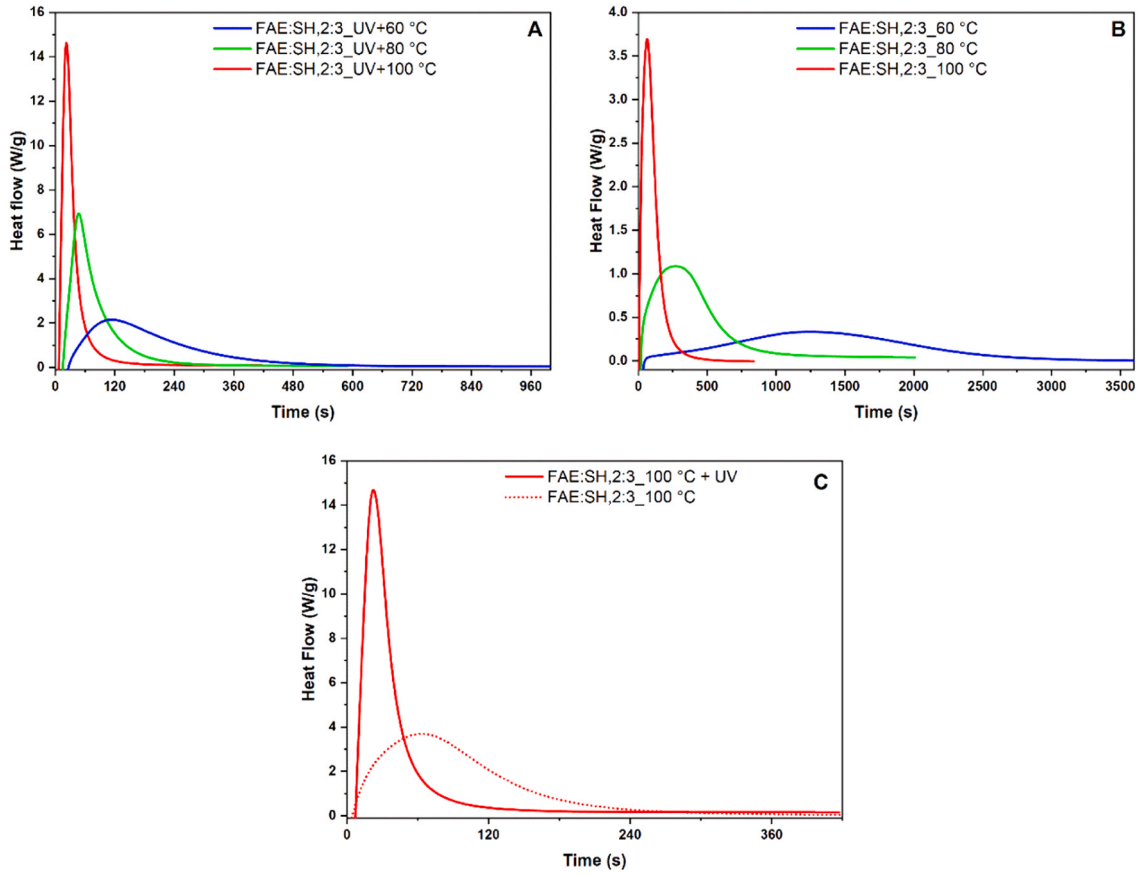


**Fig. 5.** (A) Photo-DSC of FAE:SH,2:3 (stochiometric ratio between epoxy and thiol) with 2 wt% of PLB; (B) isothermal curing of FAE:SH,2:3; (C) comparison between the thermogram registered at 100 °C with UV-irradiation (solid line) and without UV-irradiation (dot line) for FAE:SH,2:3.

**Table 2**
DSC analysis of the curing of thiol-epoxy formulations in the different tested conditions.

| ENTRY | Temperature (°C) | Irradiation | $t_{peak}$ (s) | $h_{peak}$ (W/g) | $\Delta H$ (J/g) | Conversion (%) |
|---|---|---|---|---|---|---|
| FAE:SH,2:3 | 60 | - | 1290 ± 30 | 0.40 ± 0.09 | 498 ± 17 | 94 |
| | 60 | UV | 118 ± 20 | 2.18 ± 0.57 | 494 ± 20 | 94 |
| | 80 | - | 268 ± 10 | 1.26 ± 0.23 | 506 ± 25 | 96 |
| | 80 | UV | 50 ± 8 | 7.05 ± 1.63 | 486 ± 15 | 92 |
| | 100 | - | 66 ± 25 | 3.91 ± 0.68 | 492 ± 15 | 93 |
| | 100 | UV | 20 ± 2 | 14.73 ± 0.53 | 463 ± 10 | 88 |
| FAE:SH,3:3 | 60 | - | 967 ± 50 | 0.27 ± 0.04 | 383 ± 10 | 97 |
| | 60 | UV | 115 ± 30 | 1.05 ± 0.31 | 363 ± 40 | 92 |
| | 80 | - | 236 ± 25 | 0.64 ± 0.12 | 387 ± 37 | 98 |
| | 80 | UV | 46 ± 8 | 3.23 ± 0.77 | 378 ± 23 | 96 |
| | 100 | - | 80 ± 35 | 1.67 ± 0.50 | 384 ± 15 | 97 |
| | 100 | UV | 25 ± 2 | 7.87± 0.30 | 380 ± 10 | 96 |

cationic curing of epoxy systems (Castell et al., 2000; Foix et al., 2012; Mas et al., 2001). The curing was assessed by ATR-FTIR and DSC analysis. The ATR-FTIR analysis (Fig. 7) confirmed the epoxy ring-opening reaction; indeed, considering the epoxy region located at 905 and 855 $cm^{-1}$ it is possible to observe the disappearance of the epoxy bands together with the appearance of the OH signal (3450 $cm^{-1}$). Furthermore, it can be observed that C═C double bond signal (~1640 $cm^{-1}$) did not change after the thermal treatment suggesting that a pure cationic curing process occurred.

DSC analysis was performed to complete the characterization of the curing process. Dynamic and isothermal analyses were carried out to find the best conditions to ensure complete curing. The dynamic curing results are reported in Fig. 8. From this data it was possible to calculate the activation energy of the epoxy system which was found to 71.96 KJ/mol (Sbirrazzuoli and Vyazovkin, 2002; Yoo et al., 2010). The Arrhenius plot derived for the activation energy is reported in Figure S8. The value found is in accordance with literature values for different reported epoxy systems (Lee et al., 2000; Vyazovkin and Sbirrazzuoli, 1996). Furthermore, it was also possible to establish the conversion curves as a function of the temperature related various heating rates (Fig. 8B). The dynamic curing allowed to reach full conversion, however isothermal curing was also carried out to simulate, more accurately, the curing conditions in an effort to identify the optimal parameters of time and temperature for curing (Table 3).

Following, isothermal curing of the FAE_YTT system was performed at different temperature to investigate the optimization of the thermal curing process. Isothermal runs at 150, 160, 170, and 180 °C were conducted to assess the effect of temperature, Table 4 and Figure S9. As can be noticed, the highest $\Delta H$ was achieved at 170 °C therefore the thermal curing of further specimens for the mechanical characterization

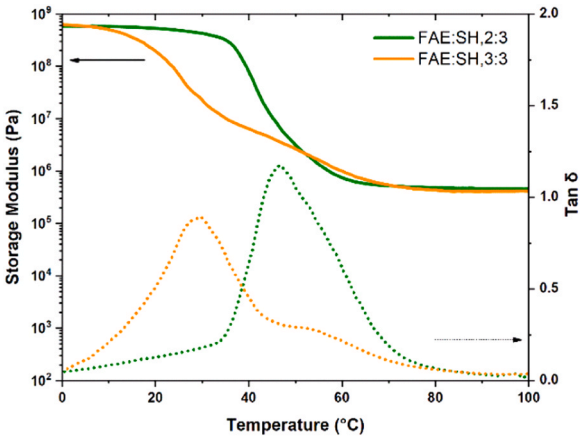


**Fig. 6.** DMTA of FAE:SH thermosets; FAE:SH,2:3 (ratio epoxy:thiol = 1:1) reported in green and FAE:SH,3:3 (ratio functional FAE group: thiol = 1:1). Y-left axis presents the storage modulus while Y-right axis shows the *Tanδ*.

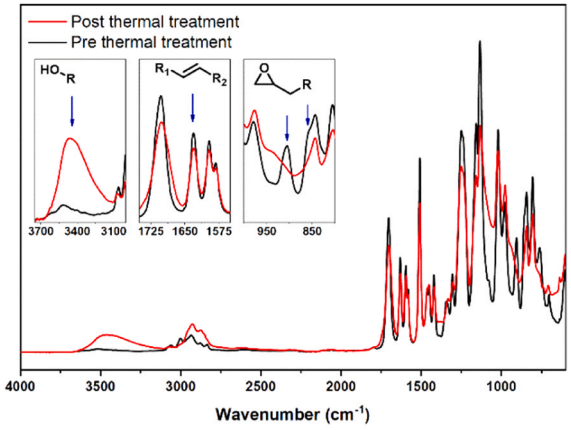


**Fig. 7.** ATR-FTIR of thermally cured FAE_YTT at 150 °C and for two hours and 180 °C for other 2 h (red line) in comparison with the uncured formulation (black line).

was performed in a two-step procedure. The curing at 150 °C was exploited to start the curing process and second step at 180 °C was used to achieve full conversion. The requirement of the second step at 180 °C was verified by performing DMTA analysis on two different samples as presented in Fig. 9. Firstly, a treatment at 150°C for 2 h was performed and the DMTA analysis showed a possible further increase in the storage modulus after the $T_g$ due to the incomplete curing achieved. Thus, applying a second stage of curing at 180 °C, we reached the highest $T_g$ possible, and the highest cross-linking density as demonstrate by the DMTA analysis with a final $T_g$ above 120 °C. The thermally cured epoxy system had the highest $T_g$ of the studied thermosets (Table 5) confirming the strong rigidity of the ferulic-based thermoset given by the aromatic structure of the monomer and the pure cationic ring opening which generate strong ether linkages. DSC was used to confirm and corroborate the $T_g$ values (Figure S10).

Finally, tensile testing was carried out of the cured thermosets to investigate the mechanical behavior at room temperature, Figure S7 and Table 5. As can be observed, the thermally cured FAE_YTT showed the highest Young's modulus and strain at break of 774 MPa and 54 MPa, respectively. This can be expected from the monomer chemistry and the cationic curing which form strong ether (C-O-C) bonds from the epoxy ring opening as aforementioned for DMTA result. Furthermore, the high $T_g$ bring a brittle behavior at room temperature as confirmed by the stress-strain curve in the tested condition.

The thermally cured system FAE_YTT revealed the best performance in terms of mechanical strength and $T_g$ with respect to the previous investigated process. Furthermore, the FAE_YTT was tested as adhesive in a shear lap test. Three different substrates were tested, a ceramic matric composite (CMC) made of C fiber reinforced Si/SiC matrix and

**Table 3**
DSC data of dynamic curing performed on FAE_YTT.

| ENTRY | ϕ (K/min) | *ΔH* (J/g) | $T_p$ (°C) | *EC* (%) |
|---|---|---|---|---|
| FAE_YTT | 2 | 413 ± 20 | 155 ± 9 | 94 |
| | 5 | 460 ± 28 | 188 ± 4 | ≈ 100 |
| | 10 | 465 ± 22 | 205 ± 2 | ≈ 100 |
| | 20 | 442 ± 28 | 211 ± 5 | ≈ 100 |

**Table 4**
Iso-curing of FAE_YTT performed at different temperatures.

| ENTRY | *Temperature* (°C) | $t_{peak}$ (s) | $h_{peak}$ (W/g) | *ΔH* (J/g) | *Conversion* (%) |
|---|---|---|---|---|---|
| FAE_YTT | 150 | 42 ± 2 | 0.42 ± 0.05 | 190 ± 20 | 43 |
| | 160 | 34 ± 2 | 0.96 ± 0.04 | 335 ± 45 | 76 |
| | 170 | 26 ± 4 | 1.15 ± 0.05 | 441 ± 30 | ≈ 100 |
| | 180 | 18 ± 4 | 1.88 ± 0.06 | 435 ± 18 | ≈ 100 |

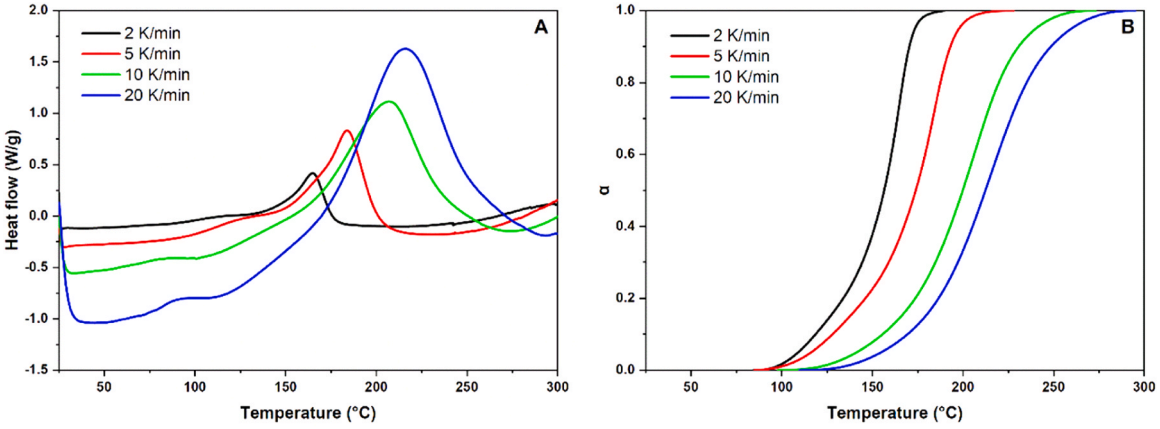


**Fig. 8.** (A) Dynamic curing of the FAE_YTT for different heating rate (2, 5, 10 and 20 K/min); (B) trend of $\alpha$ for the different heating rate in function of the temperature.

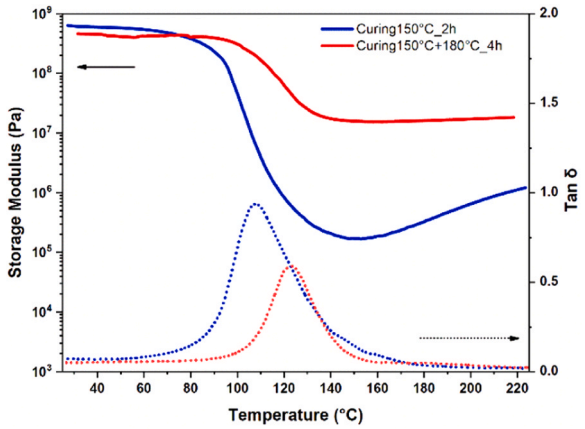


**Fig. 9.** DMTA of FAE_YTT system, left axis present the Storage Modulus while right axis presents the *Tanδ* curves in function of the temperature.

**Table 5**
Thermoset characterization performed by DMA, DSC and tensile test.

| ENTRY | $T_g$ [a] (°C) | $T_g$ [b] (°C) | $\nu$ [b] (mmol/dm$^3$) | $E$ [c] (MPa) | $\sigma$ [c] (MPa) | $\varepsilon$ [c] (%) |
|---|---|---|---|---|---|---|
| FAE: SH,2:3 | 44 ± 2 | 48 ± 2 | 58 | 250 ± 50 | 13 ± 3 | 54 ± 20 |
| FAE: SH,3:3 | 31 ± 4 | 29 ± 5 | 53 | 2.8 ± 0.3 | 1.9 ± 0.7 | 83 ± 16 |
| FAE_YTT | 117 ± 3 | 123 ± 5 | 1621 | 774 ± 30 | 25 ± 7 | 4.0 ± 1.5 |

[a] DSC analysis
[b] DMTA analysis; [c] tensile test

two metal based materials, aluminum, and steel. The typical strength vs strain curves are reported in Fig. 10 while the resulted samples after the rupture are reported in Fig. 11. Fig. 10 shows a brittle behavior of the joint, thus demonstrating the good accordance of the adhesive with common behavior of commercial epoxy-based adhesives. The metal substrates revealed a similar strength value between 20 ± 1 and 24 ± 4 MPa for aluminum and steel joint respectively. Adhesive failure at interface between substrate and epoxy adhesive was present in AISI/AISI and Al/Al as demonstrated by the resulted samples after the test. The adhesive was mostly present only on one surface meaning that the starting point of the failure was located at the interface between adhesive and substrate. Instead, as can be notice from the Fig. 10, the CMC joints revealed a cohesive failure at the adhesive the highest τ value of

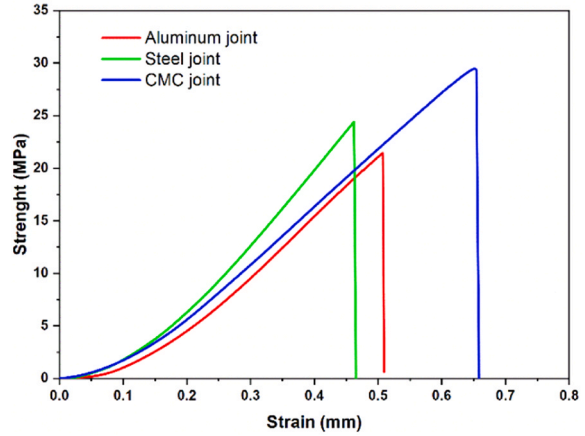


**Fig. 10.** Shear lap test curves of the FAE_YTT adhesive cured on different substrates, aluminum (red curve), steel (green line), and CMC (blue line). Representative curves are reported.

32 ± 3 MPa. Indeed, the epoxy adhesive present on both surface of the CMC and the failure must be located into the adhesive itself meaning very high adherence at the interface with the substrate. It can be speculated that the epoxy adhesive spreads on the CMC surfaces infiltrates the open porosities, thus creating a stronger interface, compared with those of adhesive with metallic substrates. In this case the failure is not due to the interface adhesive-substrate but is an adhesive failure. The τ achieved for steel and aluminum is in agreement with a previous result reported for commercially available resin (Turani et al., 2021) while the τ for the composite was higher showing a high potentiality for the bio-based epoxy derivatives in industrial applications.

Finally, the degradation of the thermosets under alkaline conditions was investigated for 2 months (Figure S11). The presence of ester bonds inside the chemical network allowed the degradation of the thermosets. The mass loss due to the hydrolysis of the thermosets was significantly different between the thermally cured epoxy and thiol-epoxy system. This can be attributed to the presence of TMPMP, which has ester bonds inside the structure increasing the possibility of degradation. For this reason, FAE:SH,3:3 degraded very quickly (4 h), while FAE:SH,2:3 needed over 200 h. Instead, the FAE_YTT thermally cured had only the ester bond proper of the ferulic acid thus its degradation was the slowest and required seven days to reach about the 60% and even after two months, traces of about 20% were still present. The result can be explained considering the highest $T_g$ of FAE_YTT which can ensure the glassy state of the network decreasing the mobility of the polymer chains and thus permeation of the degradation solution.

## 4. Conclusions

In this work, the synthesis and curing process of epoxy functionalized ferulic acid was investigated. The initial study focused on the cationic UV-curing of the bio-based synthesized epoxy monomer. However, the UV-curing allowed only partial cross-linking and incomplete formation of the network reaching a $T_g$ of about 10 °C as confirmed by ATR-FITR and DSC analysis. Thus, two different strategies were followed to overcome this problem of curing by UV-light. Firstly, a thiol monomer was introduced into the photocurable formulation, the TMPMP, promoting a photo-induced thiol-epoxy curing process in the presence of a photolatent base (PLB). The investigation of the UV-curing process highlight the effect of temperature and UV on the kinetic revealing an optimal condition for the curing at 80 °C assisted by UV-light reaching conversion over 90%. Finally, the epoxy functionalized ferulic acid was exploited in thermal cationic curing by using Ytterbium initiator. The achieved thermosets were characterized by DMTA, DSC and tensile testing. Thermally cured FAE monomer reached a $T_g$ of around 120 °C while the thermosets achieved by thiol-epoxy curing process had $T_g$ of around 30 °C and 45 °C depending on the thiol-epoxy ratio. The thermally cured FAE monomer in the presence of YTT was also exploited as adhesive. Different kinds of joints with the bio-based epoxy adhesive were manufactured and tested, showing similar or even better strength with respect to commercially available epoxy adhesives. Moreover, the currently used curing temperature of most of commercially available adhesives is unsuitable for several materials, adversely affecting their mechanical properties (i.e CFRP). In the present study, a low curing temperature and promising performance bio-based adhesive has been developed. Finally, due to the presence of ester linkages the chemical degradation was assessed revealing an effective degradation for all thermosets involved. Overall, the study demonstrated different approaches to overcome an initial problem with the opportunity of tailoring the final properties according to the monomers involved into the thermoset and the curing method adopted.

## Associated content

Supporting Information. Photorheology curves; dynamic curves of thiol-epoxy system; a fully photo-DSC analysis of FAE:SH,2:3 and FAE:

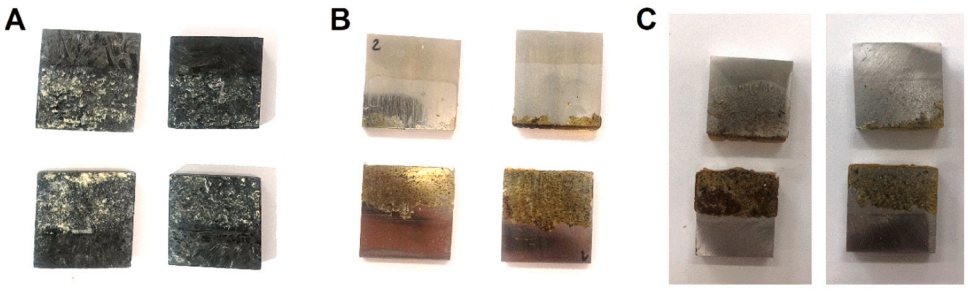


**Fig. 11.** Fracture surface of joined samples after the SLO shear test. (A) CMC composite; (B) steel and (C) aluminum. The fractured half of the joint are displayed vertically for each sample.

SH,3:3; DSC curves of cured samples; tensiles test analysis; Arrhenius plot; isocuring performed at different temperature for FAE_YTT; DSC thermogram of FAE_YTT; degradation curves.

## CRediT authorship contribution statement

**Marco Sangermano:** Funding acquisition, Conceptualization. **Lorenzo Pezzana:** Formal analysis. **Valentina Casalegno:** Data curation. **Eva Malmström:** Conceptualization. **Mats Johansson:** Conceptualization.

## Declaration of Competing Interest

The authors declare that they have no known competing financial interests or personal relationships that could have appeared to influence the work reported in this paper.

## Data availability

Data will be made available on request.

## Acknowledgements

This paper is part of a project that has received funding from the European Union's Horizon 2020 research and innovation program under the Marie Skłodowska-Curie grant agreement, No 101085759 (SURE-Poly). This study was partially carried out within the Agritech National Research Center and received funding from the European Union Next-GenerationEU (PIANO NAZIONALE DI RIPRESA E RESILIENZA (PNRR)—MISSIONE 4 COMPONENTE 2, INVESTIMENTO 1.4—D.D. 1032 17/06/2022, CN00000022).

## Appendix A. Supporting information

Supplementary data associated with this article can be found in the online version at doi:10.1016/j.indcrop.2024.118304.

## References

Alén, R., 2015. Pulp Mills and Wood-Based Biorefineries, Industrial Biorefineries and White Biotechnology. Elsevier B.V. https://doi.org/10.1016/B978-0-444-63453-5.00003-3.

Alexakis, A.E., Ayyachi, T., Mousa, M., Olsén, P., Malmström, E., 2023. 2-methoxy-4-vinylphenol as a biobased monomer precursor for thermoplastics and thermoset polymers. Polymers (Basel). https://doi.org/10.3390/polym15092168.

Auvergne, R., Caillol, S., David, G., Boutevin, B., Pascault, J.P., 2014. Biobased thermosetting epoxy: present and future. Chem. Rev. 114, 1082–1115. https://doi.org/10.1021/cr3001274.

Belmonte, A., Guzmán, D., Fernández-Francos, X., De la Flor, S., 2015. Effect of the network structure and programming temperature on the shape-memory response of thiol-epoxy "click" systems. Polymers (Basel). https://doi.org/10.3390/polym7101505.

Bozell, J.J., Petersen, G.R., 2010. Technology development for the production of biobased products from biorefinery carbohydrates—the US Department of Energy's "Top 10" revisited. Green. Chem. 12, 539–554. https://doi.org/10.1039/B922014C.

Caillol, S., Boutevin, B., Auvergne, R., 2021. Eugenol, a developing asset in biobased epoxy resins. Polymer (Guildf.) 223. https://doi.org/10.1016/j.polymer.2021.123663.

Carioscia, J.A., Stansbury, J.W., Bowman, C.N., 2007. Evaluation and control of thiol–ene/thiol–epoxy hybrid networks. Polymer (Guildf.) 48, 1526–1532. https://doi.org/10.1016/j.polymer.2007.01.044.

Castell, P., Galià, M., Serra, A., Salla, J.M., Ramis, X., 2000. Study of lanthanide triflates as new curing initiators for DGEBA. Polymer (Guildf.) 41, 8465–8474. https://doi.org/10.1016/S0032-3861(00)00275-5.

Çavuşoğlu, K., Yalçin, E., 2023. Spectral shift supported epichlorohydrin toxicity and the protective role of sage. Environ. Sci. Pollut. Res. 30, 1374–1385.

Cazacu, G., Capraru, M., Popa, V.I., 2012. Advances Concerning Lignin Utilization in New Materials. https://doi.org/10.1007/978-3-642-20940-6_8.

Chavan, P., Singh, A.K., Kaur, G., 2018. Recent progress in the utilization of industrial waste and by-products of citrus fruits: a review. J. Food Process Eng. 41, 1–10. https://doi.org/10.1111/jfpe.12895.

Chen, G.F., 1992. Developments in the field of rosin chemistry and its implications in coatings. Prog. Org. Coat. 20, 139–167. https://doi.org/10.1016/0033-0655(92)80002-E.

Chen, L., Zheng, Y., Meng, X., Wei, G., Dietliker, K., Li, Z., 2020. Delayed thiol-epoxy photopolymerization: a general and effective strategy to prepare thick composites. ACS Omega 5, 15192–15201. https://doi.org/10.1021/acsomega.0c01170.

Criado, J.M., Málek, J., Ortega, A., 1989. Applicability of the master plots in kinetic analysis of non-isothermal data. Thermochim. Acta 147, 377–385. https://doi.org/10.1016/0040-6031(89)85192-5.

de Oliveira, D.M., Finger-Teixeira, A., Rodrigues Mota, T., Salvador, V.H., Moreira-Vilar, F.C., Correa Molinari, H.B., Craig Mitchell, R.A., Marchiosi, R., Ferrarese-Filho, O., dos Santos, W., 2015. Ferulic acid: a key component in grass lignocellulose recalcitrance to hydrolysis. Plant Biotechnol. J. 13, 1224–1232. https://doi.org/10.1111/pbi.12292.

Decker, C., 2002. Kinetic study and new applications of UV radiation curing. Macromol. Rapid Commun. 23, 1067–1093. https://doi.org/10.1002/marc.200290014.

Eid, N., Ameduri, B., Boutevin, B., 2021. Synthesis and properties of furan derivatives for epoxy resins. ACS Sustain. Chem. Eng. 9, 8018–8031. https://doi.org/10.1021/acssuschemeng.0c09313.

Fang, D., Xue, D., Liu, X., Cao, L., Zhang, J., Gong, C., 2023. Concurrent production of ferulic acid and glucose from wheat bran by catalysis of a putative bifunctional enzyme. Bioresour. Technol. 369, 128393 https://doi.org/10.1016/j.biortech.2022.128393.

Feng, Y., Hu, Y., Man, L., Yuan, T., Zhang, C., Yang, Z., 2019. Biobased thiol-epoxy shape memory networks from gallic acid and vegetable oils. Eur. Polym. J. 112, 619–628. https://doi.org/10.1016/j.eurpolymj.2018.10.025.

Fernández-Francos, X., Konuray, A.-O., Belmonte, A., De la Flor, S., Serra, À., Ramis, X., 2016. Sequential curing of off-stoichiometric thiol–epoxy thermosets with a custom-tailored structure. Polym. Chem. 7, 2280–2290. https://doi.org/10.1039/C6PY00099A.

Foix, D., Ramis, X., Sangermano, M., Serra, A., 2012. Synthesis of a new hyperbranched-linear-hyperbranched triblock copolymer and its use as a chemical modifier for the cationic photo and thermal curing of epoxy resins. J. Polym. Sci. Part A Polym. Chem. 50, 1133–1142. https://doi.org/10.1002/pola.25872.

Fonseca, A.C., Lima, M.S., Sousa, A.F., Silvestre, A.J., Coelho, J.F.J., Serra, A.C., 2019. Cinnamic acid derivatives as promising building blocks for advanced polymers: Synthesis, properties and applications. Polym. Chem. 10, 1696–1723. https://doi.org/10.1039/c9py00121b.

Gandini, A., 2008. Polymers from renewable resources: a challenge for the future of macromolecular materials. Macromolecules 41, 9491–9504. https://doi.org/10.1021/ma801735u.

Gandini, A., Belgacem, N.M., 1998. Recent advances in the elaboration of polymeric materials derived from biomass components. Polym. Int. 47, 267–276 https://doi.org/10.1002/(sici)1097-0126(199811)47:3<267::aid-pi9>3.3.co;2-o.

Gandini, A., Lacerda, T.M., 2015. From monomers to polymers from renewable resources: recent advances. Prog. Polym. Sci. 48, 1–39. https://doi.org/10.1016/j.progpolymsci.2014.11.002.

Guzmán, D., Ramis, X., Fernández-Francos, X., De la Flor, S., Serra, A., 2018. Preparation of new biobased coatings from a triglycidyl eugenol derivative through thiol-epoxy click reaction. Prog. Org. Coat. 114, 259–267. https://doi.org/10.1016/j.porgcoat.2017.10.025.

Guzmán, D., Ramis, X., Fernández-Francos, X., De la Flor, S., Serra, A., 2017. New bio-based materials obtained by thiol-ene/thiol-epoxy dual curing click procedures from eugenol derivates. Eur. Polym. J. 93, 530–544. https://doi.org/10.1016/j.eurpolymj.2017.06.026.

Guzmán, D., Ramis, X., Fernández-Francos, X., Serra, A., 2015. Preparation of click thiol-ene/thiol-epoxy thermosets by controlled photo/thermal dual curing sequence. RSC Adv. 5, 101623–101633. https://doi.org/10.1039/C5RA22055F.

Ioannidou, S.M., Pateraki, C., Ladakis, D., Papapostolou, H., Tsakona, M., Vlysidis, A., Kookos, I.K., Koutinas, A., 2020. Sustainable production of bio-based chemicals and polymers via integrated biomass refining and bioprocessing in a circular bioeconomy context. Bioresour. Technol. 307, 123093 https://doi.org/10.1016/j.biortech.2020.123093.

Jha, A., Kumar, A., 2019. Biobased technologies for the efficient extraction of biopolymers from waste biomass. Bioprocess Biosyst. Eng. 42, 1893–1901. https://doi.org/10.1007/s00449-019-02199-2.

Jin, K., Heath, W.H., Torkelson, J.M., 2015. Kinetics of multifunctional thiol-epoxy click reactions studied by differential scanning calorimetry: effects of catalysis and functionality. Polymer (Guildf.) 81, 70–78. https://doi.org/10.1016/j.polymer.2015.10.068.

John, G., Nagarajan, S., Vemula, P.K., Silverman, J.R., Pillai, C.K.S., 2019. Natural monomers: a mine for functional and sustainable materials – occurrence, chemical modification and polymerization. Prog. Polym. Sci. 92, 158–209. https://doi.org/10.1016/j.progpolymsci.2019.02.008.

Kissinger, H.E., 1957. Reaction kinetics in differential thermal analysis. Anal. Chem. 29, 1702–1706.

Konuray, A.O., Fernández-Francos, X., Ramis, X., 2017a. Analysis of the reaction mechanism of the thiol–epoxy addition initiated by nucleophilic tertiary amines. Polym. Chem. 8, 5934–5947. https://doi.org/10.1039/C7PY01263B.

Konuray, A.O., Fernández-Francos, X., Ramis, X., 2017b. Latent curing of epoxy-thiol thermosets. Polymer (Guildf.) 116, 191–203. https://doi.org/10.1016/j.polymer.2017.03.064.

Konuray, O., Areny, N., Morancho, J.M., Fernández-Francos, X., Serra, À., Ramis, X., 2018. Preparation and characterization of dual-curable off-stoichiometric amine-epoxy thermosets with latent reactivity. Polymer (Guildf.) 146, 42–52. https://doi.org/10.1016/j.polymer.2018.05.040.

Konuray, O., Fernández-Francos, X., De la Flor, S., Ramis, X., Serra, À., 2020. The use of click-type reactions in the preparation of thermosets. Polymers (Basel). https://doi.org/10.3390/polym12051084.

Kreye, O., Tóth, T., Meier, M.A.R., 2011. Copolymers derived from rapeseed derivatives via ADMET and thiol-ene addition. Eur. Polym. J. 47, 1804–1816. https://doi.org/10.1016/j.eurpolymj.2011.06.012.

Kugler, S., Ossowicz, P., Malarczyk-Matusiak, K., Wierzbicka, E., 2019. Advances in rosin-based chemicals: the latest recipes, applications and future trends. Molecules 24. https://doi.org/10.3390/molecules24091651.

Kumar, N., Pruthi, V., 2014. Potential applications of ferulic acid from natural sources. Biotechnol. Rep. 4, 86–93. https://doi.org/10.1016/j.btre.2014.09.002.

Lee, J.Y., Choi, H.K., Shim, M.J., Kim, S.W., 2000. Kinetic studies of an epoxy cure reaction by isothermal DSC analysis. Thermochim. Acta 343, 111–117. https://doi.org/10.1016/S0040-6031(99)00303-2.

Llevot, A., Grau, E., Carlotti, S., Grelier, S., Cramail, H., 2016. From lignin-derived aromatic compounds to novel biobased polymers. Macromol. Rapid Commun. 37, 9–28. https://doi.org/10.1002/marc.201500474.

Ma, S., Webster, D.C., Jabeen, F., 2016. Hard and flexible, degradable thermosets from renewable bioresources with the assistance of water and ethanol. Macromolecules 49, 3780–3788. https://doi.org/10.1021/acs.macromol.6b00594.

Mas, C., Serra, A., Mantecón, A., Salla, J.M., Ramis, X., 2001. Study of lanthanide triflates as new curing initiators for cycloaliphatic epoxy resins. Macromol. Chem. Phys. 202, 2554–2564 https://doi.org/https://doi.org/10.1002/1521-3935(20010801)202:12<2554::AID-MACP2554>3.0.CO;2-C.

Ménard, R., Caillol, S., Allais, F., 2017. Ferulic acid-based renewable esters and amides-containing epoxy thermosets from wheat bran and beetroot pulp: chemo-enzymatic synthesis and thermo-mechanical properties characterization. Ind. Crops Prod. 95, 83–95. https://doi.org/10.1016/j.indcrop.2016.10.016.

Mialon, L., Pemba, A.G., Miller, S.A., 2010. Biorenewable polyethylene terephthalate mimics derived from lignin and acetic acid. Green. Chem. 12, 1704–1706. https://doi.org/10.1039/c0gc00150c.

Noè, C., Hakkarainen, M., Sangermano, M., 2021. Cationic uv-curing of epoxidized biobased resins. Polymers (Basel) 13 (1), 16. https://doi.org/10.3390/polym13010089.

Pezzana, L., Melilli, G., Guigo, N., Sbirrazzuoli, N., Sangermano, M., 2023. Photopolymerization of furan-based monomers: exploiting UV-light for a new age of green polymers. React. Funct. Polym. 185, 105540 https://doi.org/10.1016/j.reactfunctpolym.2023.105540.

Pezzana, L., Melilli, G., Guigo, N., Sbirrazzuoli, N., Sangermano, M., 2022a. Cross-linking of biobased monofunctional furan epoxy monomer by two steps process, UV irradiation and thermal treatment. Macromol. Chem. Phys., 2200012 https://doi.org/10.1002/macp.202200012.

Pezzana, Lorenzo, Melilli, G., Nathanaël, G., Sbirrazzuoli, N., Sangermano, M., 2021. Cationic UV curing of bioderived epoxy furan-based coatings: tailoring the final properties by in situ formation of hybrid network and addition of monofunctional monomer. ACS Sustain. Chem. Eng. https://doi.org/10.1021/acssuschemeng.1c06939.

Pezzana, L., Mousa, M., Malmström, E., Johansson, M., Sangermano, M., 2021. Bio-based monomers for UV-curable coatings: allylation of ferulic acid and investigation of photocured thiol-ene network. Prog. Org. Coat. 150, 105986 https://doi.org/10.1016/j.porgcoat.2020.105986.

Pezzana, L., Sangermano, M., 2021. Fully biobased UV-cured thiol-ene coatings. Prog. Org. Coat. 157, 106295.

Pezzana, L., Wolff, R., Melilli, G., Guigo, N., Sbirrazzuoli, N., Stampfl, J., Liska, R., Sangermano, M., 2022b. Hot-lithography 3D printing of biobased epoxy resins. Polymer (Guildf.) 254, 125097. https://doi.org/10.1016/j.polymer.2022.125097.

Pion, F., Ducrot, P.H., Allais, F., 2014. Renewable alternating aliphatic-aromatic copolyesters derived from biobased ferulic acid, diols, and diacids: sustainable polymers with tunable thermal properties. Macromol. Chem. Phys. 215, 431–439. https://doi.org/10.1002/macp.201300702.

Rajesh Banu, J., Preethi, Kavitha, S., Tyagi, V.K., Gunasekaran, M., Karthikeyan, O.P., Kumar, G., 2021. Lignocellulosic biomass based biorefinery: a successful platform towards circular bioeconomy. Fuel 302, 121086. https://doi.org/10.1016/j.fuel.2021.121086.

Reisinger, D., Dietliker, K., Sangermano, M., Schlögl, S., 2022. Streamlined concept towards spatially resolved photoactivation of dynamic transesterification in vitrimeric polymers by applying thermally stable photolatent bases. Polym. Chem. 13, 1169–1176. https://doi.org/10.1039/D1PY01722E.

Romano, A., Roppolo, I., Giebler, M., Dietliker, K., Možina, Š., Šket, P., Mühlbacher, I., Schlögl, S., Sangermano, M., 2018. Stimuli-responsive thiol-epoxy networks with photo-switchable bulk and surface properties. RSC Adv. 8, 41904–41914. https://doi.org/10.1039/C8RA08937J.

Rosazza, J.P.N., Huang, Z., Dostal, L., Volm, T., Rousseau, B., 1995. Biocatalytic transformations of ferulic acid: an abundant aromatic natural product. J. Ind. Microbiol. 15, 472–479. https://doi.org/10.1007/BF01570017.

Sangermano, M., Cerrone, M., Colucci, G., Roppolo, I., Acosta Ortiz, R., 2010. Preparation and characterization of hybrid thiol-ene/epoxy UV–thermal dual-cured systems. Polym. Int. 59, 1046–1051. https://doi.org/10.1002/pi.2822.

Sangermano, M., Razza, N., Crivello, J.V., 2014. Cationic UV-curing: Technology and applications. Macromol. Mater. Eng. 299, 775–793. https://doi.org/10.1002/mame.201300349.

Sbirrazzuoli, N., Vyazovkin, S., 2002. Learning about epoxy cure mechanisms from isoconversional analysis of DSC data. Thermochim. Acta 388, 289–298. https://doi.org/10.1016/S0040-6031(02)00053-9.

Silau, H., Garcia, A.G., Woodley, J.M., Dam-Johansen, K., Daugaard, A.E., 2022. Bio-based epoxy binders from lignin derivatized with epoxidized rapeseed fatty acids in bimodal coating systems. ACS Appl. Polym. Mater. 4, 444–451. https://doi.org/10.1021/acsapm.1c01351.

Silvestre, A.J.D., Gandini, A., 2008a. Terpenes: major sources, properties and applications. Monomers, Polym. Compos. Renew. Resour. 17–38. https://doi.org/10.1016/B978-0-08-045316-3.00002-8.

Silvestre, A.J.D., Gandini, A., 2008b. Rosin: major sources, properties and applications. Monomers, Polym. Compos. Renew. Resour. 67–88. https://doi.org/10.1016/B978-0-08-045316-3.00004-1.

Stanford, J.L., Ryan, A.J., Yang, Y., 2001. Photoinitiated cationic polymerization of epoxides. Polym. Int. 50, 986–997. https://doi.org/10.1002/pi.730.

Sternberg, J., Sequerth, O., Pilla, S., 2021. Green chemistry design in polymers derived from lignin: review and perspective. Prog. Polym. Sci. 113, 101344 https://doi.org/10.1016/j.progpolymsci.2020.101344.

Stuparu, M.C., Khan, A., 2016. Thiol-epoxy "click" chemistry: application in preparation and postpolymerization modification of polymers. J. Polym. Sci. Part A Polym. Chem. 54, 3057–3070. https://doi.org/10.1002/pola.28195.

Turani, M., Baggio, A., Casalegno, V., Salvo, M., Sangermano, M., 2021. An epoxy adhesive crosslinked through radical-induced cationic frontal polymerization. Macromol. Mater. Eng. 306, 2100495 https://doi.org/10.1002/mame.202100495.

Uraji, M., Kimura, M., Inoue, Y., Kawakami, K., Kumagai, Y., Harazono, K., Hatanaka, T., 2013. Enzymatic production of ferulic acid from defatted rice bran by using a combination of bacterial enzymes. Appl. Biochem. Biotechnol. 171, 1085–1093. https://doi.org/10.1007/s12010-013-0190-6.

Vyazovkin, S., Sbirrazzuoli, N., 1996. Mechanism and kinetics of epoxy−amine cure studied by differential scanning calorimetry. Macromolecules 29, 1867–1873. https://doi.org/10.1021/ma951162w.

Wilbon, P.A., Chu, F., Tang, C., 2013. Progress in renewable polymers from natural terpenes, terpenoids, and rosin. Macromol. Rapid Commun. 34, 8–37. https://doi.org/10.1002/marc.201200513.

Xin, J., Li, M., Li, R., Wolcott, M.P., Zhang, J., 2016. Green epoxy resin system based on lignin and tung oil and its application in epoxy asphalt. ACS Sustain. Chem. Eng. 4, 2754–2761. https://doi.org/10.1021/acssuschemeng.6b00256.

Yagci, Y., Jockusch, S., Turro, N.J., 2010. Photoinitiated polymerization: advances, challenges, and opportunities. Macromolecules 43, 6245–6260. https://doi.org/10.1021/ma1007545.

Ye, J., Ma, S., Wang, B., Chen, Q., Huang, K., Xu, X., Li, Q., Wang, S., Lu, N., Zhu, J., 2021. High-performance bio-based epoxies from ferulic acid and furfuryl alcohol: synthesis and properties. Green. Chem. 23, 1772–1781. https://doi.org/10.1039/D0GC03946B.

Yoo, M.J., Kim, S.H., Park, S.D., Lee, W.S., Sun, J.-W., Choi, J.-H., Nahm, S., 2010. Investigation of curing kinetics of various cycloaliphatic epoxy resins using dynamic thermal analysis. Eur. Polym. J. 46, 1158–1162. https://doi.org/10.1016/j.eurpolymj.2010.02.001.

Yue, X., Queneau, Y., 2022. 5-Hydroxymethylfurfural and furfural chemistry toward biobased surfactants. ChemSusChem 1–14. https://doi.org/10.1002/cssc.202102660, 202102660.

Zhong, L., Hao, Y., Zhang, J., Wei, F., Li, T., Miao, M., Zhang, D., 2022. Closed-loop recyclable fully bio-based epoxy vitrimers from ferulic acid-derived hyperbranched epoxy resin. Macromolecules 55, 595–607. https://doi.org/10.1021/acs.macromol.1c02247.